MM Science Journal | www.mmscience.eu
ISSN 1803-1269 (Print) | ISSN 1805-0476 (Online)
Special Issue | HSM 2023
17th International Conference on High Speed Machining
October 25-28, 2023, Nanjing, China
DOI: 10.17973/MMSJ.2023_11_2023121

HSM2023-00058

A JOINT WEARABLE STRUCTURAL REINFORCING DEVICE FOR VIBRATION SUPPRESSION IN ROBOTIC MILLING

Shihao Xin[1], Fangyu Peng[1,2], Xiaowei Tang[1]*, Jiawei Wu[1], Zhaoyang Sun[1], Rong Yan[1]

[1]Huazhong University of Science and Technology, School of Mechanical Science and Engineering, Wuhan 430074, China

[2]Huazhong University of Science and Technology, State Key Laboratory of Digital Manufacturing Equipment and Technology, Wuhan 430074, China

*Corresponding author; e-mail: txwysxf@126.com

Abstract
The structural vibration caused by poor rigidity is one of the main obstacles limiting the machining efficiency of robot milling. The existing vibration suppression strategies mainly focus on process parameter optimization, passive vibration absorption at the end and feedback control of joint motor. Although these strategies have certain vibration suppression effects, they cannot directly improve the structural rigidity of the robot. In this paper, a joint wearable structural reinforcing device (JWSRD) is proposed, which can achieve vibration suppression effect by improving the rigidity of the robot joints, fundamentally improve the processing ability of the robot, and ensure the processing stability. Firstly, the structure of the device is designed without affecting the processing flexibility. Secondly, the braking torque of the JWSRD is tested. Considering the feedback of joint braking torque, the vibration simulation model under harmonic excitation is derived. Finally, the offset mass experiments are carried out to verify the vibration suppression effect of the JWSRD. The results show that the JWSRD installed on the robot joint has the notable potential to enhance the structural rigidity, reduce the machining vibration and improve the machining efficiency.

Keywords:
Structural reinforcing, Vibration suppression, Robot structure, Wearable equipment, Robotic milling

1 INTRODUCTION

With the progress of robotic machining dynamics, pose planning and deformation control, robotic milling has become an important means of milling [1-3]. It has high processing flexibility, large working space, low cost and convenient multi-sensor integration. Exploring the processing potential of robotic milling has become the research interest of scholars in this field [4]. However, while robotic milling has many advantages, it also has significant shortcomings. Weak structural rigidity will can cause large low-frequency vibration [5] and even prone to chatter [6]. At present, the weak rigidity of robot is still the main barrier limiting its machining efficiency [7].

There are many kinds of vibration in robotic milling, and the high-frequency vibration is mainly caused by the tool structure [8]. Ultrasonic assisted vibration and other vibration suppression devices for the spindle end can be used for active vibration control of the tool structure to improve the milling stability. Gao et al. [9] developed a 3DOF ultrasonic vibration tool holder and modeled chip thickness considering the tool's rigid body motion, regenerative and ultrasonic vibration amplitude, and analyzed the stability of synchronized elliptical vibration assisted milling from the perspective of dynamics. The research shows that 3DOF ultrasonic vibration tool holder can significantly improve the machining stability under partial machining parameters. Sun et al. [10] adopted robotic rotary ultrasonic milling technology to suppress machining vibration, established an analysis model of dynamic chip thickness, and considered the influence of ultrasonic vibration on dynamic chip thickness, derived a cutting force model, and realized stability prediction. The experimental results show that the robotic milling stability area is improved by 133% when the robot rotary ultrasonic milling technology is adopted. Furthermore, the longitudinal-torsional ultrasonic milling [11, 12] is applied in vibration suppression of robotic milling based on robotic rotary ultrasonic milling technology and achieves a good vibration suppression effect.

The vibration suppression equipment for the tool structure can better suppress high-frequency vibration and even high-frequency chatter. However, the weak rigidity of the robot mainly causes relatively obvious low-frequency vibration or even low-frequency chatter, which originates from the robotic structure (the flexibility is mainly concentrated in the robot joints [13]). Vibration suppression should pay attention to the vibration of the robotic structure. Therefore, in order to solve this potential defect, vibration suppression should be carried out around the robotic structure.

Chen et al. [14] designed a new eddy current damper installed on the spindle for chatter suppression during robotic milling. By comparing the tool tip frequency responses before and after the installation of the damper, it is found that the damper can significantly reduce the dynamic flexibility of tool modes, thus improving the stability boundary of high-frequency chatter. Yuan et al. [15] designed a magnetorheological elastomer (MRE) with adjustable stiffness in view of the low frequency of robot structure dynamic characteristics and significant pose dependence. They propose a new mode coupling chatter suppression scheme in which an MRE is installed on a spindle and a semi-active controller is established to control the current applied to the MRE to track the chatter frequency. The results show that the MRE with adjustable stiffness can track and absorb the low-frequency vibration energy well, so as to play the role of vibration suppression. Zhang et al. [16] used an inertial actuator near the robotic excitation source to generate a force to counteract vibration. In order to further improve the effectiveness and robustness of active vibration control, h∞ control strategy is established. The experimental results show that the active vibration suppression strategy of the inertia actuator can effectively improve the machining capability and reduce the machining error by 85%.

At present, although the research on vibration suppression of low-frequency vibration or chatter of robots has achieved initial results, the existing devices are mostly installed in the end-effector of robots, and vibration suppression is carried out by means of vibration absorption, without corresponding structural enhancement according to the structural characteristics of the robot. On the one hand, end-effector attachment may affect the machining flexibility of the robot, especially in aircraft segments or complex parts processing. On the other hand, the vibration suppression device installed on the end-effector of the robot only has the effect of indirect vibration absorption, which cannot directly enhance the structural rigidity, so as to play the role of vibration suppression at the root.

Therefore, this paper carried out structural enhancement based on wearable equipment for the joint structure in the weak link of the robot structure, so as to improve the resistance ability of the robot structure to processing vibration, fundamentally improve the robot's processing ability and ensure the processing stability. The rest of the paper is structured as follows: In Section 2, a joint wearable structural reinforcing device (JWSRD) is developed for robotic torsional joints about 2, 3 and 5, and its mechanical properties are analyzed. In Section 3, considering the suppression of the device, a joint braking coefficient for the evaluation of braking effect was established. Based on this, the suppression effect of JWSRD on robot end vibration under harmonic excitation was analyzed by simulation. In Section 4, the experimental verification of vibration suppression effect is carried out by using offset mass experiment. Section 5 summarizes the full paper and describes the future work.

2 DEVELOPMENT OF JOINT WEARABLE STRUCTURAL REINFORCING DEVICE

2.1 Structure design of JWSRD

In this study, ABB IRB6660 robot was used as the experimental platform. ABB IRB6660 robot has two joint types, one such as 2, 3 and 5 joints, which are characterized by the two links connected by the joint are intersecting, the other such as the 1, 4 and 6 joints, which are characterized by the two links connected by the joint are coaxial. The JWSRD proposed in this paper is applicable to the joint 2, 3 and 5 of the robot, which can realize the structural reinforcing of the robot joint.

Magnetorheological (MR) fluids are common types of fluids with controllable mobility, consisting of stable suspensions of magnetizable particles dispersed in a carrier medium, such as silicone oil or water. Low viscosity Newtonian fluid in the absence of an external magnetic field. When applied with magnetic field, Bingham fluid with high viscosity and low fluidity transforms from free-flowing liquid to semi-solid or even solid within milliseconds, showing strong controllable rheological properties [17]. The viscosity of liquid corresponds to the magnetic flux, and the change is rapid, reversible and controllable. In this paper, a drum type magnetorheological damper (MRD) was used to design JWSRD according to the 2, 3 and 5 joint structures of ABB IRB6660, so as to realize the structural reinforcing of robot joints. The proposed design of JWSRD is aimed at suppressing the vibration of robotic joints, as shown in Fig. 1, the specific structural design of JWSRD for joint 3. The specific structure of the MRD used by JWSRD is shown in Fig. 1. (c). When energized to generate a magnetic field, JWSRD will generate a braking torque that impedes joint vibration, and the maximum torque is positively correlated with the current. The JWSRD structure of each joint is shown in Fig. 2.

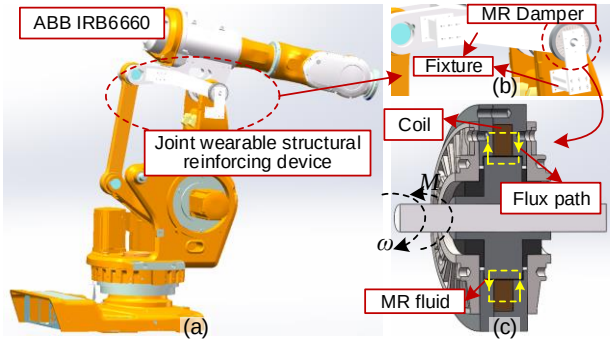

Fig. 1: JWSRD design schematic.

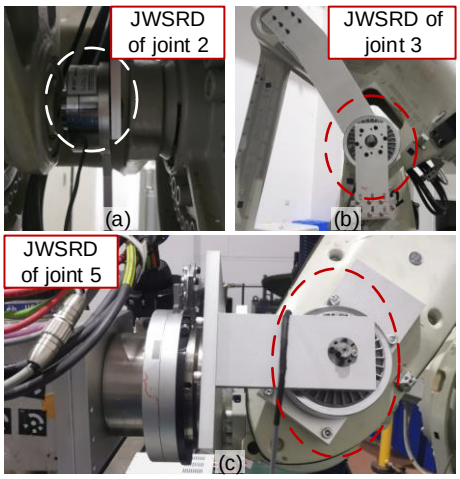

Fig. 2: JWSRD structure of each joint.

2.2 Analysis and modeling of JWSRD braking torque

As shown in Fig. 1. (c), MRD mainly consists of MR fluid, magnetic coil, rotor and stator. The inner diameter of the cavity filled with MR fluid r_1 = 35mm, the outer diameter r_2 = 35.5mm, and the effective width of MR fluid w = 7.5mm. The damping force of JWSRD can be calculated according to the structural parameters of MRD [17]. When there is no external magnetic field, MR fluid presents the characteristics of low viscosity Newtonian fluid. At this time, the braking torque T_0 of JWSRD is expressed as follows:

$$T_\omega = \frac{4\pi\eta w r_1^2 r_2^2 \omega}{r_2^2 - r_1^2} \tag{1}$$

while η = 0.28Pa·S is the viscosity of the MR fluid without magnetic field and ω is the rotational speed of the rotor.

When the magnetic coil is energized, the MR fluid appears as a Bingham fluid with variable yield strength, and the strength of the magnetic field determines its yield strength. In this case, the braking torque T of JWSRD is calculated as follows:

$$T = T_B + T_\omega = \frac{4\pi w \tau_B r_1^2 r_2^2 \ln(r_2/r_1)}{r_2^2 - r_1^2} + \frac{4\pi\eta w r_1^2 r_2^2 \omega}{r_2^2 - r_1^2} \tag{2}$$

while τ_B is the yield stress produced by the external magnetic field, and the size of τ_B is related to magnetic induction intensity B, and the size of magnetic induction intensity is related to the size of magnetic coil current I. The relation between the yield stress τ_B generated by MRD under the influence of external magnetic field and current I is shown in Tab. 1. The mathematical relationship between the two can be obtained by fitting, as shown in Fig. 3. The expression is as follows:

$$\tau_B = -161.8596I^3 + 135.4288I^2 + 228.4023I - 5.7226 \tag{3}$$

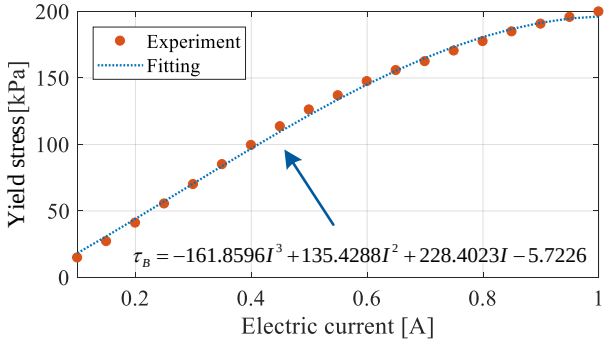

Fig. 3: The fitting result of yield stress and current magnitude.

Tab. 1: Yield stress at different electric currents.

Index	1	2	3	4	5	6	7	8	9	10	11
Electric current (A)	0	0.1	0.2	0.3	0.4	0.5	0.6	0.7	0.8	0.9	1.0
Yield stress (KPa)	0	14.7	40.9	69.9	99.3	126	147.3	162.3	177.4	190.5	199.7

The braking torque of JWSRD after energizing is composed of two parts. T_B is the minimum torque of its rotation, and its magnitude is related to the magnitude of energized current, but independent of rotation. T_ω is the viscous damping of torsional degrees of freedom generated by the viscosity of MR fluid after its rotation.

By Eq.(2) and JWSRD design size can calculate the braking torque changes, such as Fig. 4 for braking torque when the input current is 0.5 A trend along with the change of angular velocity. At 0~7.149Nm, JWSRD does not rotate. When the joint force is greater than T_B = 7.149Nm, JWSRD begins to vibrate with joint vibration, and the braking torque changes with the angular velocity of joint vibration.

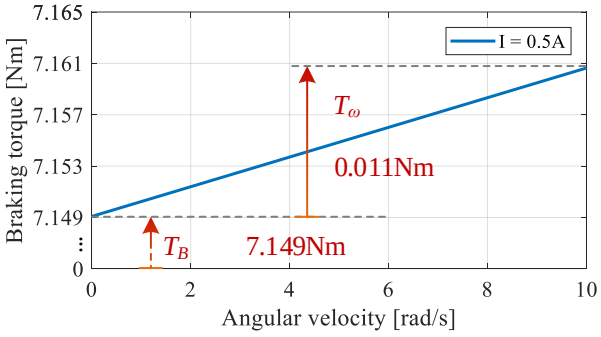

Fig. 4: Change of braking torque with angular velocity.

Taking the current I = 0.1−1.0A as an example, the braking torque of JWSRD is simulated according to Eq. (2) . In order to verify the correctness of the theoretical calculation of braking torque, the braking torque is tested under the same parameters. The test platform is shown in Fig. 5, the test results are shown in Tab. 2, and the theoretical calculation and measured results are compared in Fig. 6. The results show that the experiment is in good agreement with the theoretical calculation, and the calculation formula Eq. (2) of braking torque can accurately reflect the actual braking torque.

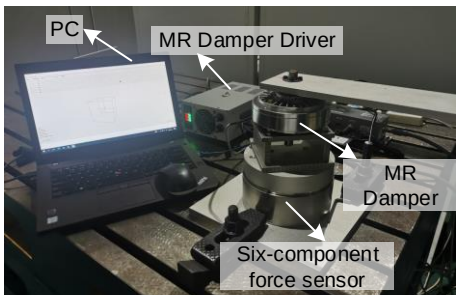

Fig. 5: Brake torque test platform.

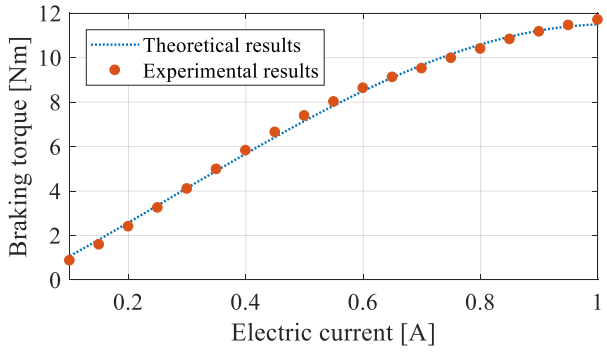

Fig. 6: Comparison of theoretical and experimental results.

Tab. 2: Barking torque at different electric currents.

Index	1	2	3	4	5	6	7	8	9	10	11
Electric current (A)	0	0.1	0.2	0.3	0.4	0.5	0.6	0.7	0.8	0.9	1.0
Barking torque (Nm)	0.17	0.87	2.40	4.09	5.82	7.38	8.62	9.51	10.39	11.16	11.70

3 JOINT BRAKE COEFFICIENT DERIVATION AND ROBOT END VIBRATION SIMULATION

3.1 Joint braking coefficient under JWSRD

According to the structural characteristics of the robot, the kinematics model was established by D-H method, and the force Jacobian matrix was obtained, so as to realize the mapping from the end of the exciting force to the joint space. According to the D-H method, considering its parallel four-link mechanism, the link coordinate system is established, as shown in Fig. 7, and D-H parameters are shown in Tab. 3. Based on the link coordinate system in Fig. 7, the Jacobian matrix **J**(q) is calculated by using the cross-product method.

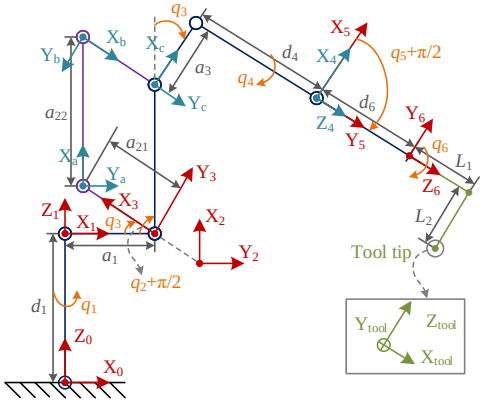

Fig. 7: Robotic link coordinate system.

In robotic milling, the exciting force and vibration at the end will be transferred to the joint, thus causing the overall structure of the robot to vibrate, which is manifested as low-frequency vibration or even low-frequency chatter [5]. The vibration velocity and exciting force of the robot end can be mapped to the joint space through the Jacobian matrix, as shown below:

$$\begin{cases} \mathbf{q}_v = \mathbf{J}^{-1}(q)\mathbf{v}_e \\ \mathbf{M}(t) = \mathbf{J}_F(q)\mathbf{F}(t) \end{cases} \tag{4}$$

where $\mathbf{J}_F(q) = \mathbf{J}^T(q)$ is the Force Jacobian matrix, $\mathbf{q}_v = [q_{v,1}, q_{v,2}, q_{v,3}, q_{v,4}, q_{v,5}, q_{v,6}]^T$ represents the vibration velocity of each joint, $\mathbf{v}_e = [v_{e,x}, v_{e,y}, v_{e,z}, v_{e,\omega x}, v_{e,\omega y}, v_{e,\omega z}]^T$ represents the linear and rotational vibration velocity of the x, y, and z direction of the robot end, $\mathbf{M}(t) = [M_1(t), M_2(t), M_3(t), M_4(t), M_5(t), M_6(t)]^T$ is the torque of each joint, and $\mathbf{F}(t) = [F_x(t), F_y(t), F_z(t), M_x(t), M_y(t), M_z(t)]^T$ represents the exciting force and torque of the robot end in three directions.

As a passive vibration suppression device with Bingham fluid characteristics, JWSRD will rotate only when the torque applied reaches the critical value of its minimum shear stress, otherwise it will behave as an ordinary elastic body. When the joint is the absolute value of torque $|M_i(t)|$ not greater than the braking torque T, joints affected by JWSRD without vibration, the actual joint vibration velocity $\tilde{q}_{v,i}(t) = 0$. When the absolute value of the torque $|M_i(t)|$ exerted on the joint is greater than the braking torque T, JWSRD rotates, and the braking torque is related to the rotation speed, as shown in Eq. (2). At this time, the equivalent force on the joint is $|M_i(t)| - T$, and the direction of braking torque T is opposite to the direction of the force on the joint $M_i(t)$, and is always less than or equal to the force on the joint. When the dynamic characteristics of the system are unchanged, the vibration velocity of the joint is proportional to the force on the joint, and the actual vibration velocity of the joint decreases proportionally to the equivalent force exerted on the joint. The attenuation rate $\alpha_{q,i}$ is related to the torque exerted on the joint $M_i(t)$ and braking torque T, which is hereinafter referred to as the joint braking coefficient, expressed as follows:

$$\alpha_{q,i} = \begin{cases} \dfrac{|M_i(t)| - T}{|M_i(t)|} & |M_i(t)| > T \\ 0 & |M_i(t)| \le T \end{cases}, \quad i = 1 \sim 6 \tag{5}$$

Therefore, considering the braking effect of JWSRD, the actual joint vibration can be calculated as follows:

$$\tilde{q}_{v,i}(t) = q_{v,i}(t)\alpha_{q,i}, \quad i = 1 \sim 6 \tag{6}$$

Tab. 3: D-H parameters of robot (ABB IRB6660).

Link i	d_i (mm)	a_{i-1} (mm)	α_{i-1} (rad)	θ_i (rad)
1	0	0	814.5	q_1
2	300	-π/2	0	q_2 - π/2
3	0	0	0	q_3 - q_2 - π/2
a	500	0	0	q_2 - q_3 + π/2
b	700	0	0	q_3 - q_2 + π/2
c	500	0	0	-π/2
4	280	-π/2	893	q_4
5	0	π/2	0	q_5
6	0	-π/2	200	q_6 – π/2

3.2 Simulation of robot end vibration suppression under harmonic excitation based on joint brake coefficient

Considering the joint braking coefficient expression of JWSRD as shown in Eq.(5), the joint braking coefficient represents the braking effect of JWSRD on the vibration of each joint under any posture. In order to evaluate the end vibration suppression effect of JWSRD, a simulation model of end vibration suppression should be established based on the joint braking coefficient.

The corrected joint vibration velocity can be mapped to the end of the robot through the Jacobian matrix, so as to obtain the real end vibration velocity. The expression is as follows:

$$\tilde{\mathbf{v}}_e = \mathbf{J}(q)\tilde{\mathbf{q}}_v \tag{7}$$

where $\tilde{\mathbf{v}}_e = \left[\tilde{v}_{e,x}, \tilde{v}_{e,y}, \tilde{v}_{e,z}, \tilde{v}_{e,\omega x}, \tilde{v}_{e,\omega y}, \tilde{v}_{e,\omega z}\right]^{\mathrm{T}}$ represents the linear and rotational vibration velocity of the robot end of x, y, and z directions considering the braking effect of JWSRD, and $\tilde{\mathbf{q}}_v = \left[\tilde{q}_{v,1}, \tilde{q}_{v,2}, \tilde{q}_{v,3}, \tilde{q}_{v,4}, \tilde{q}_{v,5}, \tilde{q}_{v,6}\right]^{\mathrm{T}}$ represents the vibration velocity of each joint considering the braking effect of JWSRD.

In order to verify the suppression effect of JWSRD on the robot end vibration, a harmonic excitation force $\mathbf{F}_e(t)$ = $[A_e\sin(2\pi f_e t), A_e\cos(2\pi f_e t), 0, 0, 0, 0]^{\mathrm{T}}$ with amplitude A_e and frequency f_e is assumed to be applied to the robot end. Joint force expression can be obtained by simultaneous Eq.(4) as follows:

$$\mathbf{M}(t) = \mathbf{J}_F(q)\mathbf{F}_e(t) = A_e \begin{bmatrix} j_{F,11} & j_{F,12} \\ j_{F,12} & j_{F,22} \\ j_{F,13} & j_{F,23} \\ j_{F,14} & j_{F,24} \\ j_{F,15} & j_{F,25} \\ j_{F,16} & j_{F,26} \end{bmatrix} \begin{bmatrix} \sin(2\pi f_e t) \\ \cos(2\pi f_e t) \end{bmatrix} \tag{8}$$

The braking torque expression is shown in Eq.(2). As shown in Fig. 4, the viscous damping of the JWSRD is very small. For the convenience of analysis and calculation, the influence of this term is ignored. Combined Eq.(2) −Eq.(8), it can be seen that the robot end vibration velocity $\tilde{\mathbf{v}}_e$ considering JWSRD is a function of resultant direction (time), amplitude and frequency of harmonic excitation force, robot posture, current magnitude, and robot end vibration velocity $\mathbf{v}_e$ without considering JWSRD. Braking effect can be expressed as follows:

$$\mathbf{A} = \frac{\tilde{\mathbf{v}}_e}{\mathbf{v}_e} = \begin{bmatrix} \alpha_x & \alpha_y & \alpha_z & \alpha_{\omega x} & \alpha_{\omega y} & \alpha_{\omega z} \end{bmatrix} \tag{9}$$

where, α_i(i = x, y, z, ωx, ωy, ωz) represents the braking coefficient in each direction under the action of JWSRD, and is a function of the resultant direction, the amplitude and frequency of the harmonic excitation force, the robot attitude and the current magnitude.

In order to verify the braking effect of JWSRD, the parameters shown in Tab. 4 are brought into the simulation calculation, and the robot configuration is shown in Tab. 5. The braking coefficient varying with the direction of resultant force under harmonic excitation is shown in Fig. 8. Fig. 8. (a) shows the variation law of three-way braking coefficient of Group B, and Fig. 8. (b) shows the variation law of three-way braking coefficient of Group D. In fact, since the direction of the resultant cutting force changes all the time in milling, the braking coefficient which changes with the resultant force direction in Fig. 8 does not have a clear guiding significance in milling. In order to guide processing, the average braking coefficient within a changing period is used to represent the braking effect under the simulation parameters. The braking effect of Group B is obtained as α_x = 0.6383, α_y = 0.8076, α_z = 0.5385. The braking effect of Group D is α_x = 0.8700, α_y = 0.9447, α_z = 0.8251.

Tab. 4: Simulation parameters.

Index	Spindle speed (Rpm)	Electric current (A)
Group A	600	0
Group B		0.8
Group C	1200	0
Group D		0.8

Tab. 5: Robot configuration.

Axis 1 (°)	Axis 2 (°)	Axis 3 (°)	Axis 4 (°)	Axis 5 (°)	Axis 6 (°)
28.23	4.83	48.24	35.72	-54.07	-22.88

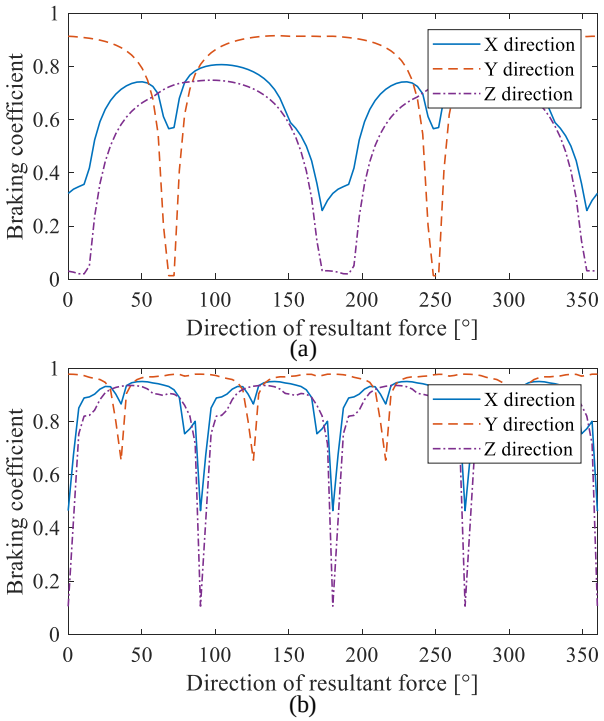

Fig. 8 : Braking coefficient varying with the direction of resultant force. (a) Spindle speed = 600rpm, (b) Spindle speed = 1200rpm.

4 EXPERIMENTAL VERIFICATION OF VIBRATION SUPPRESSION EFFECT BASED ON OFFSET MASS EXPERIMENT

Based on the simulation results of Section 3.2, offset mass experiments were carried out in this section to further verify the vibration suppression effect of JWSRD. In the experiment, a rotating offset mass is attached to the end-effector of the robot to achieve the specified harmonic excitation, and then the robot is induced to vibrate. The offset mass is 0.072kg, and the offset distance is 25.0mm. When the spindle rotates at a constant speed, there will be a centripetal force acting on the spindle of a certain magnitude. The force can be modeled as a sine wave with respect to a fixed reference frame, whose period is the spindle speed period. 3D scanning laser Doppler vibrometer (Polytec PSV-500-3D-H) was used to test vibration signals in the experiment. Experimental settings are shown in Fig. 9.

The offset mass experiment adopts the spindle speed of 600rpm and 1200rpm respectively, corresponding to the excitation frequency of 10Hz and 20Hz respectively. The robotic configuration is shown in Tab. 5. In the experiment,

the robot end vibration signals of JWSRD under energized and unenergized states were respectively tested, and the measuring point was set on the actuator. According to the simulation prediction results, the Z-direction vibration suppression effect was the most obvious, so the Z-direction test results were taken as an example to analyze the experimental results. The Z-direction vibration velocity signal of the robot end obtained from the test is shown in Fig. 10, where Fig. 10. (a) are the experimental results under the parameters Group A and Group B, and Fig. 10. (b) are the experimental results under the parameters Group C and Group D. In order to observe the end vibration suppression effect of JWSRD more clearly, the frequency domain signal of the robot end of Z-direction vibration displacement signal was tested, as shown in Fig. 11.

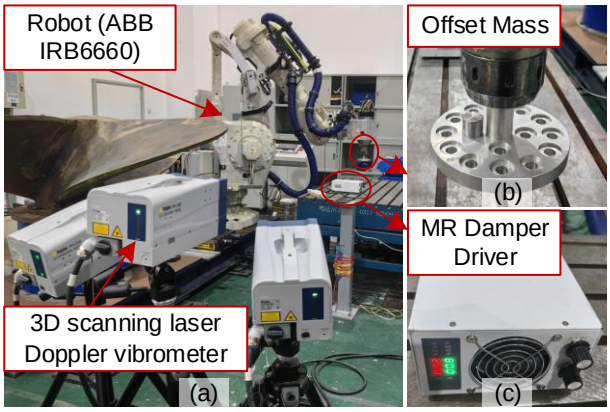

Fig. 9: Experimental settings.

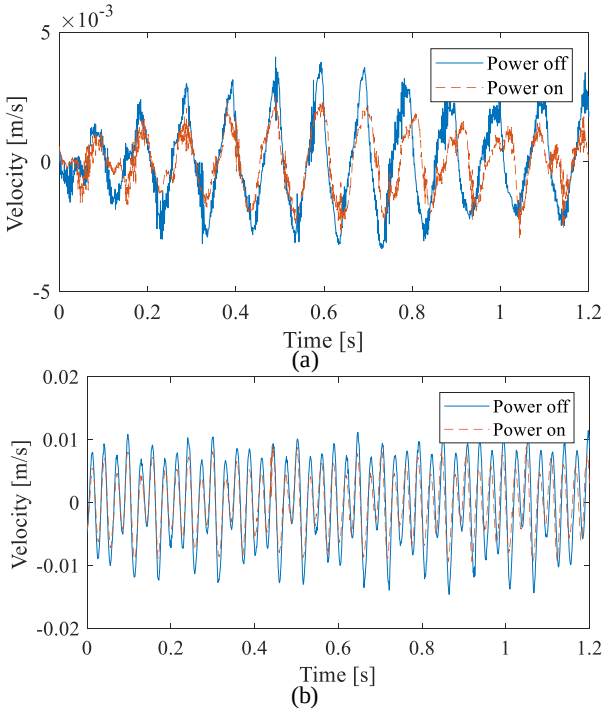

Fig. 10: Z-direction vibration velocity signal of the robot end. (a) Group A and B, (b) Group C and D.

As can be seen from Fig. 11. (a), there is only a vibration frequency of 10Hz in the vibration spectrum at 600rpm, which is consistent with the excitation frequency. By comparing the vibration test results with and without JWSRD enabled, it can be seen that the forced vibration of the system can be effectively suppressed, with a vibration suppression ratio of about 40.08%. At this time, the braking coefficient is 0.5991, which is close to the predicted result (α_z = 0.5385). It can be seen from Fig. 11. (b) that there are multiple vibration frequencies in the vibration spectrum at 1200rpm, where the forced vibration frequency is 20Hz, 15Hz is the modal frequency of the robot excited by harmonic excitation at this time, and 35Hz is the sideband frequency arising from the modulation between the forced vibration frequency and the modal frequency [5, 18]. It can be seen that JWSRD has a certain suppression effect on all types of vibration, the vibration suppression ratio is about 22.64%, and the braking coefficient is 0.7736, which is close to the predicted result (α_z = 0.8251).

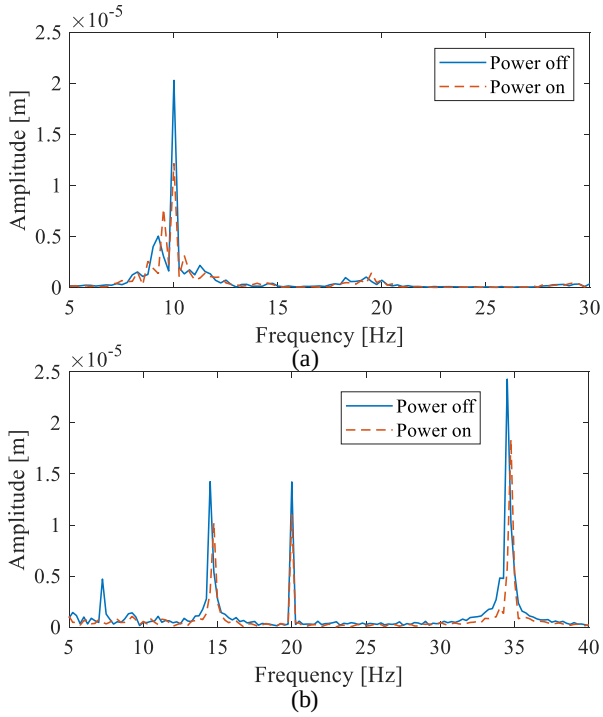

Fig. 11: Z-direction vibration displacement spectrum signal of the robot end. (a) Group A and B, (b) Group C and D.

To sum up, JWSRD can play a certain role in suppressing vibration regardless of whether the system modal frequency is excited by external excitation sources, and it has a certain consistency with the conclusion of the simulation analysis model. Experiments show that JWSRD installed on robot joints has the potential to enhance structural rigidity, reduce machining vibration and improve machining efficiency. The proposed simulation model also has a certain accuracy, which can provide theoretical guidance for optimization of vibration suppression effect.

5 CONCLUSION AND FUTURE WORK

In this paper, a JWSRD based on MRD is proposed, which is used to enhance the rigidity of robot structure and suppress vibration. Simulation and experiments show that the device can suppress all kinds of vibration, including forced vibration and excited modal frequency vibration. Based on the research in this paper, the following conclusions can be drawn:

1. The vibration suppression effect of JWSRD has a strong correlation with the excitation direction and frequency, and the experiment shows that JWSRD is better at the suppression of low-frequency vibration.
2. When the modal frequency is excited and there are both forced vibration and self-excited vibration, JWSRD still has a good vibration suppression effect,

and the amplitude of forced vibration and self-excited vibration is observed to decrease in the experiment.

3. The proposed device does not affect the flexibility of the robot and can be used as a new idea to enhance the stiffness of the robot structure.

Further research and experimental verification are needed to analyze the relationship between JWSRD vibration suppression effect and robot configuration and current magnitude, the optimization of JWSRD vibration suppression effect dependent on robot configuration, and the effectiveness analysis of JWSRD in milling, which will be carried out in the future work, so as to extend JWSRD to vibration suppression in robotic milling.

6 ACKNOWLEDGMENTS

This research is supported by the National Natural Science Foundation of China under Grant No. 52175463, National Natural Science Foundation of China under Grant No. 52005201, and National Natural Science Foundation of China under Grant No. 52188102.

7 REFERENCES

[1] [Zhu 2021] Z. Zhu, X. Tang, C. Chen, F. Peng, R. Yan, L. Zhou, Z. Li, J. Wu, High precision and efficiency robotic milling of complex parts: Challenges, approaches and trends, Chinese Journal of Aeronautics, 2021, 35, 2, pp 22-46, ISSN 1000-9361.

[2] [Verl 2019] A. Verl, A. Valente, S. Melkote, C. Brecher, E. Ozturk, L.T. Tunc, Robots in machining, Cirp Annals-Manufacturing Technology, 2019, 68, pp 799-822, ISSN 0007-8506.

[3] [Iglesias 2015] I. Iglesias, M.A. Sebastián, J.E. Ares, Overview of the State of Robotic Machining: Current Situation and Future Potential, Procedia Engineering, 2015, 132, pp 911-917, ISSN 1877-7058.

[4] [Yuan 2017] L. Yuan, S. Sun, Z. Pan, D. Ding, W. Li, Ieee, Semi-Active Chatter Reduction for Robotic Machining Using Magnetorheological Elastomers (MBEs), in: 7th IEEE Annual International Conference on CYBER Technology in Automation, Control, and Intelligent Systems (CYBER), Honolulu, HI, 2017, pp. 349-354, ISBN 978-1-5386-0490-8.

[5] [Xin 2022] S. Xin, F. Peng, X. Tang, R. Yan, Z. Li, J. Wu, Research on the influence of robot structural mode on regenerative chatter in milling and analysis of stability boundary improvement domain, International Journal of Machine Tools and Manufacture, 2022, 179, pp 103918, ISSN 0890-6955.

[6] [Pan 2006] Z.X. Pan, H. Zhang, Z.Q. Zhu, J.J. Wang, Chatter analysis of robotic machining process, Journal of Materials Processing Technology, 2006, 173, pp 301-309, ISSN 0924-0136.

[7] [Ji 2019] W. Ji, L.H. Wang, Industrial robotic machining: a review, International Journal of Advanced Manufacturing Technology, 2019, 103, pp 1239-1255, ISSN 0268-3768.

[8] [Xin 2022] S.H. Xin, F.Y. Peng, C. Chen, X.W. Tang, R. Yan, Z.P. Li, J.W. Wu, Chip wave phase difference analysis of robotic milling and chatter dominant mode research, International Journal of Advanced Manufacturing Technology, 2022, 122, pp 1431-1455, ISSN 0268-3768.

[9] [Gao 2020] J. Gao, Y. Altintas, Chatter stability of synchronized elliptical vibration assisted milling, CIRP J. Manuf. Sci. Technol., 2020, 28, pp 76-86, ISSN 1755-5817.

[10] [Sun 2020] L.J. Sun, K. Zheng, W.H. Liao, J.S. Liu, J.D. Feng, S. Dong, Investigation on chatter stability of robotic rotary ultrasonic milling, Robotics and Computer-Integrated Manufacturing, 2020, 63, 101911, ISSN 0736-5845.

[11] [Zhang 2022] J.L. Zhang, W.H. Liao, W. Zhao, W. Tian, K. Zheng, B. Li, Research on stability of robotic longitudinal-torsional ultrasonic milling with variable cutting force coefficient, International Journal of Advanced Manufacturing Technology, 2022, 121, pp 1707-1715, ISSN 0268-3768.

[12] [Sun 2022] L.J. Sun, W.H. Liao, K. Zheng, W. Tian, J.S. Liu, J.D. Feng, Stability analysis of robotic longitudinal-torsional composite ultrasonic milling, Chinese Journal of Aeronautics, 2022, 35, pp 249-264, ISSN 1000-9361.

[13] [Wu 2022] J.W. Wu, F.Y. Peng, X.W. Tang, R. Yan, S.H. Xin, X.Y. Mao, Characterization of milling robot mode shape and analysis of the weak parts causing end vibration, Measurement, 2022, 203, 14, pp 111934, ISSN 0263-2241.

[14] [Chen 2018] F. Chen, H. Zhao, Design of eddy current dampers for vibration suppression in robotic milling, Advances in Mechanical Engineering, 2018, 10, 11, pp 1-15, ISSN 1687-8132.

[15] [Yuan 2019] L. Yuan, S. Sun, Z. Pan, D. Ding, O. Gienke, W. Li, Mode coupling chatter suppression for robotic machining using semi-active magnetorheological elastomers absorber, Mechanical Systems and Signal Processing, 2019, 117, pp 221-237, ISSN 0888-3270.

[16] [Zhang 2022] R.N. Zhang, Z. Wang, P. Keogh, H-infinity optimised control of external inertial actuators for higher precision robotic machining, International Journal of Computer Integrated Manufacturing, 2022, 35, pp 129-144, ISSN 0951-192X.

[17] [Huang 2002] J. Huang, J.Q. Zhang, Y. Yang, Y.Q. Wei, Analysis and design of a cylindrical magneto-rheological fluid brake, Journal of Materials Processing Technology, 2002, 129, pp 559-562, ISSN 0924-0136.

[18] [Wang 2018] L.M. Wang, Y.M. Shao, Z. Cao, Optimal demodulation subband selection for sun gear crack fault diagnosis in planetary gearbox, Measurement, 2018, 125, pp 554-563, ISSN 0263-2241.